

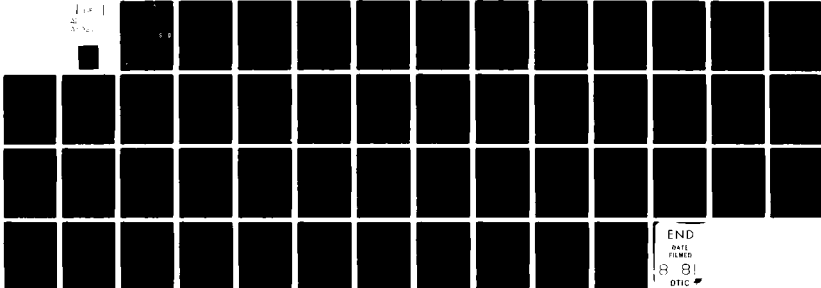
AD-A102 201

AIR FORCE INST OF TECH WRIGHT-PATTERSON AFB OH
F/G 20/1
VISCIOUS AND THERMAL EFFECTS ON RESONANT PHOTO-ACOUSTIC SPECTROS--ETC(U)
DEC 79 W J KOENITZER
AFIT-CI-79-274T

UNCLASSIFIED

NL

1 of 1
3/82



END
DATE
FILMED
8 81
DTIC

UNCLASS

SECURITY CLASSIFICATION OF THIS PAGE (When Data Entered)

LEVEL II

①

REPORT DOCUMENTATION PAGE

READ INSTRUCTIONS BEFORE COMPLETING FORM

1. REPORT NUMBER 79-274T		2. GOVT ACCESSION NO. AD-A102201		3. RECIPIENT'S CATALOG NUMBER	
4. TITLE (and Subtitle) Viscous and Thermal Effects on Resonant Photo-Acoustic Spectroscopy,				5. TYPE OF REPORT & PERIOD COVERED THESIS/DISSERTATION/	
				6. PERFORMING ORG. REPORT NUMBER	
7. AUTHOR(s) Lt. William J. Koenitzer				8. CONTRACT OR GRANT NUMBER(s)	
9. PERFORMING ORGANIZATION NAME AND ADDRESS AFIT STUDENT AT: Princeton University				10. PROGRAM ELEMENT PROJECT, TASK AREA & WORK UNIT NUMBERS 15	
11. CONTROLLING OFFICE NAME AND ADDRESS AFIT/NR WPAFB OH 45433				12. REPORT DATE December 1979	
14. MONITORING AGENCY NAME & ADDRESS (if different from Controlling Office) 147				13. NUMBER OF PAGES 44	
				15. SECURITY CLASS. (of this report) UNCLASS	
15a. DECLASSIFICATION/DOWNGRADING SCHEDULE					
16. DISTRIBUTION STATEMENT (of this Report) APPROVED FOR PUBLIC RELEASE; DISTRIBUTION UNLIMITED					
17. DISTRIBUTION STATEMENT (of the abstract entered in Block 20, if different from Report)					
18. SUPPLEMENTARY NOTES APPROVED FOR PUBLIC RELEASE: IAW AFR 190-17				<p style="text-align: center;">E</p> <p style="text-align: center;"><i>Fredric C. Lynch</i></p> <p style="text-align: center;">FREDRIC C. LYNCH, Major, USAF Director of Public Affairs Air Force Institute of Technology (ATO) Wright-Patterson AFB, OH 45433</p>	
19. KEY WORDS (Continue on reverse side if necessary and identify by block number)					
20. ABSTRACT (Continue on reverse side if necessary and identify by block number) ATTACHED					

AD A 102201

DTIC FILE COPY

23 JUN 1981

VISCOUS AND THERMAL EFFECTS ON
RESONANT PHOTO-ACOUSTIC SPECTROSCOPY

by

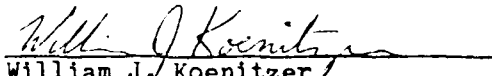
William J. Koenitzer

Princeton University
School of Engineering and Applied Science
Mechanical and Aerospace Engineering Department

Accession For	
NTIS GRA&I	<input checked="" type="checkbox"/>
DTIC TAB	<input type="checkbox"/>
Unannounced	<input type="checkbox"/>
Justification	
By _____	
Distribution/ _____	
Availability Codes	
Dist	Avail and/or Special
A	

Submitted in partial fulfillment of the requirements for the degree of
Master of Science in Engineering from Princeton University, 1979.

Prepared by:


William J. Koenitzer

Approved by:

Professor George K. Bienkowski

December, 1979

81 7 28 031

PREFACE

As I am completing my work, I would like to take time to thank everyone who contributed to my stay at Princeton University. First, thanks to the U. S. Air Force for allowing me to go on to school, and the Guggenheim Fellowship Committee for funding my studies. Thanks to my advisor, Prof. G. K. Sienkowski, for giving me some much needed direction, and providing the idea for and guidance throughout my thesis research. Thanks to Dr. Jack Gelfand for his patience in introducing me to that strange world of experimental science. Finally, thanks to all the other instructors, staff members, and students who were, in one way or another, a part of my Princeton experience. The studies were challenging, the research was interesting, and the whole experience was very rewarding.

This thesis carries No. T-1478 in the records of the Department of Mechanical and Aerospace Engineering.

TABLE OF CONTENTS

PREFACE ii
LIST OF SYMBOLS iv
ABSTRACT. vi
1. INTRODUCTION. 1
2. EQUATIONS OF MOTION 5
3. BOUNDARY CONDITIONS 11
4. EIGENVALUES 16
5. EXPERIMENT. 24
6. CONCLUSIONS 29
APPENDIX A. 32
APPENDIX B. 33
REFERENCES. 43

LIST OF SYMBOLS

a = radius of cylinder	$\alpha = \left(\frac{\partial \rho}{\partial T} \right)_V$
c = speed of sound	$\gamma = \text{ratio of specific heats, } C_p/C_v$
$C_p = \text{specific heat at constant pressure}$	$\delta = \text{density variation}$ $= \text{logarithmic decrement}$
$C_v = \text{specific heat at constant volume}$	$\delta_y = \text{Dirac delta}$
d = boundary layer thickness	$\epsilon = \left(\tau \sqrt{\lambda_n k} \right)^{-1}$
f = frequency (cycles/sec)	$\eta = \text{bulk modulus}$
h = Planck's constant	$\theta = \text{azimuthal coordinate}$
k = eigenvalue	$K = \text{thermal conductivity}$
l = characteristic length, approx. mean free path	$K_s = \frac{1}{\gamma \rho} \left(\frac{\partial \rho}{\partial P} \right)_T$
L = length of cylinder	$\mu = \text{coefficient of viscosity}$
m = azimuthal index	$\nu = \text{light frequency}$
n = radial index	$\zeta = \text{acoustic impedance}$
O = on the order of	$\pi = 3.14159\dots$
p = pressure variation = longitudinal index	$\rho = \text{density}$
P = pressure	$\sigma = \text{entropy variation}$
Pr = Prandtl number	$\tau = \text{temperature variation}$
$Q(\omega) = \text{resonant frequency divided by half-power width}$	$\phi = \text{phase angle}$
r = radial coordinate	$\omega = \text{frequency (radians/sec)}$
S = entropy	
t = time	
T = temperature	
u = velocity	
z = longitudinal coordinate	

SUBSCRIPTS

h = thermal

l = longitudinal

o = zeroth order value

p = propagational
= constant pressure

t = transverse

T = constant temperature

v = viscous
= constant volume

\perp = perpendicular

\parallel = parallel

SUPERSCRIPTS

o = special case for $k_{r_0} = 0$, or $k_{z_0} = 0$

\sim = non-dimensional quantity

\rightarrow = vector quantity

ABSTRACT

The Photo-acoustic effect occurs when a chopped beam of light shining on an absorbing gas produces sound waves. From the amplitude of these waves one can infer the absorption spectrum of a known sample, or detect trace gases in an unknown sample. While the signal strength is inversely proportional to the sample chamber volume, in some cases it is advantageous to design a large cell as an acoustic resonance chamber, and modulate the excitation beam at a natural frequency of the chamber. The resonant amplification factor $Q(\omega)$ depends upon the system losses. The dominating loss mechanisms are the thermal and viscous boundary layer effects. By rescaling the local coordinates, one can include these losses, neglecting terms smaller than the boundary layer thickness, simply by modifying the boundary conditions for the non-dissipative wave equation. From there one can derive an equation for $Q(\omega)$ applicable at all sample chamber resonances. This equation will be useful in evaluating the relative advantages of resonant and non-resonant photo-acoustic spectroscopy.

An experiment conducted with a Krypton/Argon laser shining on a one atmosphere sample of dry air with .5% NO_2 enclosed in a cylinder resulted in amplification factors less than those predicted. An analysis of the data, and the results of later experiments at lower pressures indicated that the unpredicted losses were probably due to imperfect cell construction.

AK

81 7 28 031

Chapter 1: INTRODUCTION

In 1880 Alexander Graham Bell discovered the photo-acoustic effect whereby light energy is converted into sound. He found that intensity modulated light focused on a solid substance enclosed in a sample cell produced audible sound. Later, both Tyndall and Bell observed similar results shining light through sample cells containing gasses and liquids. The light energy passing through a rotating light chopper is periodically absorbed by the irradiated molecules, and rereleased as heat causing a periodic pressure pulse, or sound wave. The energy absorbed is greatest when the light energy ($h\nu$) equals one of the energy transitions within the irradiated molecules.

Fifty years after Bell's discovery, Viengrov used the photo-acoustic effect to construct the first gas concentration measurement instrument, and to record the first absorption spectra. When he tuned the incident light to a single wavelength, the intensity of the resulting acoustic signal was proportional to the concentration of molecules in the sample with that corresponding energy transition. When he scanned the light source across a range of wavelengths, the intensity of the acoustic signals corresponded to the absorption spectrum of the sample.¹³

In recent years, the development of lasers as sources of intense wavelength tunable light has revived interest in the photo-acoustic effect. Kerr and Atwood¹⁴ (1968) conducted the first experiments with a laser illuminated optoacoustic detector measuring the weak atmospheric absorption of laser radiation by water vapor. Kreuzer¹⁵ performed the first gas concentration measurement with a laser illuminated optoacoustic detector. The increased sensitivity of optoacoustic detectors due to the

use of lasers has made them useful in measuring atmospheric pollution concentrations in the parts per billion range, and gas absorption coefficients as low as 10^{-8} cm^{-1} . One may also use the optoacoustic detector to determine the energy transfer rates between vibrational and translational degrees of freedom in gas molecules by monitoring the phase lag between the modulated light and the pressure variation.

In most photo-acoustic experiments the sample cell is a cylinder; the laser shines along the axis of the cell; and a microphone converts the acoustic signal into an electric signal. The resulting signal amplitude is proportional to the gas absorption coefficient and the incident light intensity, but inversely proportional to the chamber cross sectional area. Sensitive acoustic cells then are usually as small in diameter as possible. Practical considerations of aligning the laser beam and accommodating commercial microphones limits typical cell diameters to 25-50mm. However, in 1973 Dewey, Kamm, and Hackett² demonstrated that in some cases one could enhance the acoustic signal using a larger diameter cell designed as an acoustic resonance chamber, and modulating the excitation beam at one of the natural frequencies of the chamber. In many cases this resonant operation is better than non-resonant operation. For example, Shumate et. al.⁵ used a resonant optoacoustic detector to measure water vapor absorption of carbon dioxide laser radiation. They needed a large volume to surface area ratio cell to minimize the effects of water vapor adsorption at the walls.

This paper provides a rigorous treatment of the problem of pressure signals produced by a distributed heat source in a cylinder. The results should be useful in improving the interpretation and design of photo-

acoustic experiments. Specifically, they can help in judging the relative merits of resonant and non-resonant cells. The results of the analysis are general equations for $Q(\omega)$ and phase shift governing all the resonances of a cylinder.

In most current photo-acoustic spectroscopy literature the emphasis is on laser light absorption and relaxation mechanisms, with only a simple analysis of the acoustics portion of the problem. Often the acoustic equations and boundary conditions used do not include any dissipation, or the system losses are determined experimentally without regard to their origin.^{2.4.5.9} While a non-dissipative analysis is adequate for predicting the approximate resonance locations, the results give physically unrealistic infinite responses at resonance. Some major sources of system dissipation are;

1. Losses due to the compliance of chamber walls
2. Dissipation at the microphone diaphragm
3. Losses from wave scattering at obstructions
4. Free space viscous and thermal losses
5. Viscous and thermal boundary layer losses
6. Relaxational losses.¹²

A sufficiently rigid cell wall material can make reflection losses due to the compliant chamber walls insignificant. Dissipation at the microphone diaphragm is similar in nature to that due to flexible walls. Consideration of microphone losses as energy dissipation alone however, is insufficient since the energy lost at the diaphragm is closely linked with the ability to detect the pressure waves. For a microphone with a small surface area compared with that of the cell, the loss is minimal.¹²

The losses due to scattering from microphone mounts and inlet ports etc., while significant, are extremely difficult to predict, and the cell design should be as smooth as possible to minimize them. The next section will show that, for typical cell dimensions and pressures, viscous and thermal losses in free space are negligible compared to viscous and thermal losses in the boundary layer. Relaxation losses occur because of the finite energy transfer rates within the absorbing molecules. The beam modulation rate must be much slower than the vibrational relaxation time of the gas to minimize these losses. Accurate predictions of dissipation due to relaxation effects depend upon precise knowledge of the energy transfer processes, and are not included in this paper.

Chapter 2 demonstrates that one can include the effects of viscosity, thermal conductivity, and compliant walls on an acoustic wave in a problem simply by modifying the boundary conditions. Chapter 3 derives these boundary conditions for a closed cylinder. Chapter 4 solves the resulting eigenvalue problem, deriving equations for the resonant frequency, the Q , and phase shift of each cylinder resonance. Chapter 5 describes an experiment conducted to verify those equations.

Chapter 2: EQUATIONS OF MOTION¹

The alternate compressions and rarefactions in a sound wave correspond to high and low temperature areas. In a gas with finite thermal conductivity, the faster high temperature molecules diffuse into the cooler regions, equalizing the temperature and lessening the amplitude of the sound wave. The fluid velocity which accompanies an acoustic wave is proportional to the gradient of pressure or temperature. Viscosity tends to equalize the fluid velocity along the wave, and to deintensify the sound. When a pressure wave strikes a wall which is not perfectly rigid, the surface reflects only part of the wave energy, and absorbs the rest. The ratio of the pressure to the normal fluid velocity at a point on a surface is the acoustic impedance of the surface.

One can describe the acoustic behavior of a fluid as the sum of three waves; a propagational wave, a thermal heat diffusion wave, and a transverse shear wave. The thermal and transverse waves will be negligible outside of thin surface boundary layers, but they will account for the majority of the wave power lost in a small container like those used in photo-acoustic spectroscopy. The thermal and shear waves appear because the propagational wave, although it dominates the acoustic behavior, cannot, by itself, satisfy the boundary conditions for temperature, tangential velocity, and normal velocity. Since the viscous and thermal boundary layers are very thin, one can consider the power loss to occur at the boundaries, and can include the compliant boundary, thermal mode, and shear mode effects simply by modifying the boundary conditions on the propagational mode.

For the small disturbances associated with acoustic waves, each of

the variables describing the fluid state consists of an equilibrium part plus a small time varying acoustic part.

$$\begin{aligned} \text{Pressure: } & P + p(x, t) & \text{Temperature: } & T + \tau(x, t) \\ \text{Density: } & \rho + \delta(x, t) & \text{Entropy/unit mass: } & S + \sigma(x, t) \\ \text{Velocity: } & \vec{u}(x, t) & & \end{aligned}$$

The linear equations governing the wave motion are:

$$\begin{aligned} (1) \quad \frac{\partial \delta}{\partial t} + \rho \nabla \cdot \vec{u} &= 0 & \text{Conservation of mass} \\ (2) \quad \rho \frac{\partial \vec{u}}{\partial t} &= -\nabla p + (\eta + \frac{2}{3}\mu) \nabla (\nabla \cdot \vec{u}) - \mu \nabla \times (\nabla \times \vec{u}) & \text{Conservation of momentum} \\ (3) \quad T \frac{\partial \sigma}{\partial t} &= K \nabla^2 \tau & \text{Continuity for heat flow} \\ (4) \quad \delta &= \partial^1 \rho K_s (p - \alpha \tau) & \text{Equation of state} \\ (5) \quad \sigma &= \frac{C_p}{T} \left(\tau - \frac{(\gamma - 1)}{\alpha \gamma} p \right) & \text{Second law of thermodynamics} \end{aligned}$$

where,

$$\begin{aligned} \mu &= \text{coefficient of viscosity} \\ \eta &= \text{bulk modulus} \\ K &= \text{thermal conductivity} \\ C_p &= \text{specific heat at constant pressure} \\ \gamma &= \text{ratio of specific heats, } C_p/C_v \\ K_s &= \frac{1}{\partial^1 \rho} \left(\frac{\partial \rho}{\partial p} \right)_T \\ \alpha &= \left(\frac{\partial p}{\partial T} \right)_v. \end{aligned}$$

Any vector function of space, such as \vec{u} , has two parts: a longitudinal part \vec{u}_l for which $\nabla \times \vec{u}_l = 0$, and a rotational or transverse part

\vec{u}_t for which $\nabla \cdot \vec{u}_t = 0$. Since $\nabla \times (\nabla p) = 0$, one can separate the Navier-Stokes momentum equation into two equations.

$$(6) \quad \rho \frac{\partial \vec{u}_t}{\partial t} = -\nabla p + (\eta + \frac{2}{3}\mu) \nabla (\nabla \cdot \vec{u}_t)$$

$$(7) \quad \rho \frac{\partial \vec{u}_t}{\partial t} = -\mu \nabla \times (\nabla \times \vec{u}_t)$$

The conservation of mass equation becomes

$$(8) \quad \frac{\partial \delta}{\partial t} + \rho \nabla \cdot \vec{u}_t = 0.$$

Equation 7 defines \vec{u}_t , which is the shear wave mentioned earlier. The shear wave is not coupled to any changes in fluid pressure or temperature.

One can use the conservation of mass equation, its first derivative with respect to time,

$$\nabla \cdot \vec{u}_t = \frac{-1}{\rho} \frac{\partial \delta}{\partial t} \quad \rho \nabla \cdot \frac{\partial \vec{u}_t}{\partial t} = - \frac{\partial^2 \delta}{\partial t^2},$$

and the definitions of ζ and σ (equations 4 and 5) to reduce the system of equations above to two equations in two unknowns, p and ζ .

$$(9) \quad \nabla^2 p = \gamma \rho K_S \left(\frac{\partial^2}{\partial t^2} - \frac{(\eta + \frac{2}{3}\mu)}{\rho} \frac{\partial}{\partial t} \nabla^2 \right) (p - \alpha \zeta)$$

$$(10) \quad \frac{K}{C_p} \nabla^2 \zeta = \frac{\partial}{\partial t} \left(\zeta - \frac{(\gamma-1)}{\alpha \gamma} p \right)$$

Equation 11 expresses the longitudinal velocity \vec{u}_l in terms of p and ζ .

$$(11) \quad \rho \frac{\partial \vec{u}}{\partial t} = -\nabla \left(p - \gamma' K_s (\eta + \frac{4}{3}\mu) \frac{\partial}{\partial t} (p - \alpha \tau) \right)$$

One can also write these equations in terms of characteristic lengths, each on the order of the molecular mean free path.

$$(12) \quad l_h \equiv \frac{k}{\rho c_p c} \quad l_v \equiv \frac{\mu}{\rho c} \quad l_v' \equiv \frac{\eta + \frac{4}{3}\mu}{\rho c}$$

$$(13) \quad \nabla^2 p = \frac{\gamma'}{c^2} \left(\frac{\partial^2}{\partial t^2} - l_v' c \frac{\partial}{\partial t} \nabla^2 \right) (p - \alpha \tau)$$

$$(14) \quad l_h c \nabla^2 \tau = \frac{\partial}{\partial t} \left(\tau - \frac{(\gamma' - 1)}{\alpha \gamma'} p \right)$$

$$(15) \quad \rho \frac{\partial \vec{u}}{\partial t} = -\nabla \left(p - \frac{\gamma' l_v'}{c} \frac{\partial}{\partial t} (p - \alpha \tau) \right)$$

These equations represent two kinds of waves depending on which equation (13 or 14) dominates. One can find the equations governing each wave by considering separable simple harmonic motion,

$$\begin{aligned} \nabla^2 p &= -k^2 p & \frac{\partial p}{\partial t} &= -i\omega p \\ \nabla^2 \tau &= -k^2 \tau & \frac{\partial \tau}{\partial t} &= -i\omega \tau \end{aligned}$$

and solving for the two solutions to the resulting quadratic in k^2 .

$$(16) \quad (l_h c - \gamma' l_h l_v' i\omega) k^4 - \left(i\omega + \frac{\gamma' l_h \omega^2}{c} + \frac{l_v' \omega^2}{c} \right) k^2 + \frac{i\omega^3}{c^2} = 0$$

One solution corresponds to nearly adiabatic motion; the propagation velocity has a real part equal to c , and a small imaginary part correspon-

ding to the energy loss terms in l_h and l'_v . This is the propagational mode, and it is governed (to first order in l_h and l'_v) by the following equations:

$$\nabla^2 p = -k^2 p \quad \frac{\partial p}{\partial t} = -i\omega p$$

$$(17a) \quad k^2 \approx \frac{\omega^2}{c^2} \left[1 + \frac{i\omega l'_v}{c} + i(\gamma-1) \frac{\omega l_h}{c} \right]$$

$$(17b) \quad \tau \approx \frac{\gamma-1}{2\gamma} \left(1 - i \frac{\omega}{c} l_h \right) p$$

$$(17c) \quad \vec{u}_e \approx \left(\frac{1}{i\omega\rho} - \frac{l'_v}{\rho c} \right) \nabla p.$$

The other value of k^2 is large and complex, indicating rapid attenuation. This wave corresponds chiefly to heat diffusion. It is the thermal mode, and is governed by:

$$\nabla^2 \tau = -k^2 \tau \quad \frac{\partial \tau}{\partial t} = -i\omega \tau$$

$$(18a) \quad k^2 \approx \frac{i\omega}{l_h c} \quad (18b) \quad p \approx \frac{i\gamma\alpha\omega}{c} (l_h - l'_v) \tau$$

$$(18c) \quad \vec{u}_e = \frac{\alpha\gamma}{\rho c} l_h \nabla \tau.$$

The plane wave solution for the thermal wave is

$$\tau = A e^{ikx - i\omega t}$$

$$\tau = A \exp \left[\sqrt{\frac{\omega}{2l_h c}} (i-1)x - i\omega t \right].$$

The thermal boundary layer thickness then is on the order of $\sqrt{\frac{2k_h c}{\omega}}$.

$$(19) \quad d_h \equiv \sqrt{\frac{2k_h c}{\omega}}$$

For the shear layer

$$u_{ty} = A e^{ikx - i\omega t}$$

$$u_{ty} = A \exp\left[\sqrt{\frac{\omega \rho}{2\mu}} (i-1)x - i\omega t\right].$$

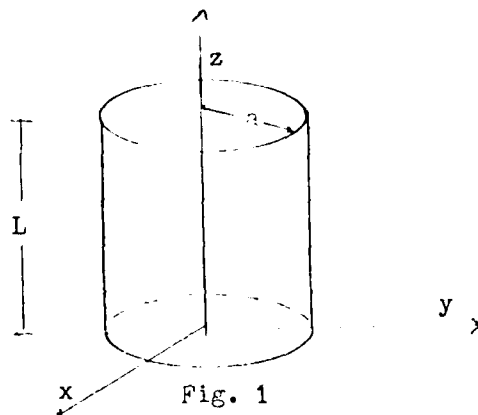
The viscous boundary layer thickness is on the order of $\sqrt{\frac{2\mu}{\rho\omega}} = \sqrt{\frac{2l_v c}{\omega}}$.

$$(20) \quad d_v \equiv \sqrt{\frac{2l_v c}{\omega}}$$

Therefore, while the propagational mode decays as $\exp(-\frac{1}{2}(\frac{\omega}{c})^2 [l_v' + (\gamma-1)l_h]x)$, the thermal and shear modes decay as $\exp(-\sqrt{\frac{\omega}{2l_h c}} x)$ and $\exp(-\sqrt{\frac{\omega}{2l_v c}} x)$. One can see that in a photo-acoustic chamber, $\frac{l_h}{a} = 0(10^{-6}, 10^{-7})$, that the thermal and shear waves exist only in a thin area near the boundaries, but account for most of the system losses. For typical photo-acoustic frequencies and chamber sizes the attenuation of the propagational mode is negligible, and one can assume all the power is lost in the boundary layer, or since the layer is so thin, at the boundary itself. Further analysis will neglect terms of order l_h and retain only those terms of the same order as the boundary layer thickness: d_v , d_h , $\sqrt{l_v}$, $\sqrt{l_h}$, and larger.

Chapter 3: BOUNDARY CONDITIONS

Consider the cylindrical configuration shown in figure 1.



The propagational mode equations are now

$$p_p = R(r) \Theta(\theta) Z(z) e^{-i\omega t}$$

$$(21a) \quad \frac{d^2 Z}{dz^2} = -k_z^2 Z \quad (21b) \quad \frac{d^2 \Theta}{d\theta^2} = -m^2 \Theta$$

$$(21c) \quad \frac{d^2 R}{dr^2} + \frac{1}{r} \frac{dR}{dr} + \left(k_r^2 - \frac{m^2}{r^2} \right) R = 0$$

$$(21d) \quad \tau_p = \frac{\gamma - 1}{\omega^2} p_p \quad (21e) \quad \vec{u}_p = \frac{1}{i\omega\rho} \nabla p_p$$

If the boundary surface is rigid the tangential and normal velocities equal zero at the surface. In the case of a slightly flexible wall one can assume the surface is one of local reaction, with acoustic impedance ζ to account for a nonnegligible velocity normal to the wall. Tangential velocity would still be negligible. The heat capacity of the boundary material is usually much greater than that of the fluid so the temperature variation τ approximately equals zero at the surface. Therefore, a

reasonable approximation to the true boundary conditions is:

$$(22) \quad u_{\perp} = \frac{-p}{\gamma} \quad u_{\parallel} = 0 \quad \tau = 0$$

at $r = a$, $z = 0$, $z = L$.

But the propagational wave cannot meet all three of these conditions and satisfy its own equation as well. One must add enough of the shear and thermal modes so that the combination wave satisfies all three conditions. A discussion below of the $r = a$ boundary will demonstrate how the other modes affect the propagational boundary conditions.

Assume that the thermal mode has the separable form

$$\tau_h = H(r) \Phi(\theta) F(z) e^{-i\omega t}$$

$$(23) \quad \nabla^2 \tau_h = \frac{-i\omega}{\chi_h c} \tau_h = \frac{-2i}{d_h^2} \tau_h$$

The substitution $r = a - d_h x$ rescales the local coordinate normal to the boundary, and enables one to eliminate terms smaller than d_h .

$$\frac{d^2 H}{dx^2} = -\lambda_c H$$

$$(24) \quad \tau_h = (b_1 e^{(1-i)x} + b_2 e^{-(1-i)x}) \Phi F e^{-i\omega t}$$

Physically the solution must decay with positive x ; so $b_1 = 0$. The thermal solution should just cancel the temperature fluctuation due to the propagational wave at $r = a$.

$$\tau_h = -\tau_p$$

This implies that

$$(25) \quad z_h = \frac{1-\gamma}{\alpha \beta^n} R(\omega) \Theta Z e^{(1-i) \frac{r-a}{d_h} - i\omega t}$$

The thermal wave has with it a corresponding velocity $\vec{u}_h = \frac{\alpha \beta^n}{\rho c} l_h \nabla z$. The θ and z components are of order d_h^2 , but the r velocity component is not negligible.

$$(26) \quad u_{h_r} = \frac{1-\gamma}{\rho c} \frac{l_h}{d_h} R(\omega) (1-i) \Theta Z e^{(1-i) \frac{r-a}{d_h} - i\omega t}$$

The shear wave will cancel the tangential velocity due to the propagational wave.

$$(27) \quad \nabla \times \nabla \times \vec{u}_t = \frac{-\rho}{\mu} \frac{\partial \vec{u}_t}{\partial t} = \frac{2i}{d_v^2} \vec{u}_t$$

Letting $r = a - d_v x$ and dropping small terms, and adjusting constants to cancel the θ and z components,

$$(28a) \quad u_{t_\theta} = \frac{-1}{i\omega \rho} \frac{1}{a} R(\omega) \frac{d\Theta}{d\theta} Z e^{(1-i) \frac{r-a}{d_h} - i\omega t}$$

$$(28b) \quad u_{t_z} = \frac{-1}{i\omega \rho} R(\omega) \Theta \frac{dZ}{dz} e^{(1-i) \frac{r-a}{d_h} - i\omega t}$$

The rotational velocity \vec{u}_t is not coupled to any changes in temperature or pressure, but it does have a component in the r direction which one finds from the definition of \vec{u}_t .

$$\nabla \cdot \vec{u}_t = 0$$

$$(29) \quad \vec{u}_{t_r} = \frac{-1}{i\omega \rho} \frac{d_v}{(1-i)} R(\omega) (\frac{m^2}{\omega^2} + k_2^2) \Theta Z e^{(1-i) \frac{r-a}{d_h} - i\omega t}$$

The thermal, shear, and propagational components of the normal fluid

velocity together must satisfy the $u_{\perp} = -p/\xi$ boundary condition.

$$(u_{rh} + u_{rp} + u_{rt}) = -p/\xi$$

Solving for u_{rp} results in the true boundary conditions for p_p .

$$(30) \quad u_{rp} = \frac{1}{i\omega\rho} \frac{\partial p_p}{\partial r} = - \left(\frac{1}{\xi} + \frac{(1-i)}{\rho c} \left[(\omega l_h) \sqrt{\frac{\omega l_h}{2c}} + \frac{(m^2 + k_z^2) c^2 \sqrt{\omega l_v}}{\omega^2} \right] \right) p_p$$

at $r = a$

The three terms within the parentheses correspond to compliant boundary, thermal conductivity, and viscosity effects respectively. Assuming the elastic boundary effects are small ($\frac{1}{\xi} = O[\sqrt{l_h}]$), equation 30 is simply the non-dissipative $\frac{\partial p}{\partial n} = 0$ boundary condition with small modifications to include losses. Since thermal losses are caused by compression which is related to the normal velocity, the thermal effect is equivalent to an additional acoustic conductance. The viscous term is more complicated. Since viscous losses are related to the tangential velocity of the fluid just outside the boundary layer, the viscous term involves eigenvalues from the other two orthogonal directions. In non-dimensional form, using the conventions below, the $r = a$ boundary condition is

$$\frac{1}{\xi} = \epsilon \sqrt{\frac{l_h}{a}} \quad \tilde{\omega} = \frac{\omega a}{c} \quad \tilde{k}_r = k_r a \quad \tilde{k}_z = k_z a$$

$$\tilde{z} = \frac{z}{a} \quad \tilde{r} = \frac{r}{a} \quad Pr = \frac{l_v}{l_h} = \text{Prandtl number} \quad \tilde{\epsilon} = c\rho\epsilon$$

$$(31) \quad \frac{\partial p}{\partial r} = - \sqrt{\frac{l_h}{a}} i\tilde{\omega} \left(\tilde{\epsilon} + (1-i) \left[(\tilde{\omega} l_h) \sqrt{\frac{\tilde{\omega}}{2}} + \frac{m^2 + \tilde{k}_z^2}{\tilde{\omega}^2} \sqrt{\frac{\omega l_v}{2}} \right] \right) p$$

at $\tilde{r} = 1$.

One can find the $z = 0$ and $z = L$ boundary conditions in a similar manner using the substitutions $z = L - d_{h,v}y$ at the $z = L$ boundary, and $z = d_{h,v}y$ at the $z = 0$ boundary. The $z = 0$ and $z = L$ boundary conditions are:

$$(32) \quad \frac{\partial \rho}{\partial \tilde{z}} = \sqrt{\frac{l_h}{a}} i\omega \left(\tilde{\epsilon} + (1-i) \left[(\gamma-1) \sqrt{\frac{\tilde{\omega}}{2}} + \frac{\tilde{k}_r^2}{\tilde{\omega}^2} \sqrt{\frac{\tilde{\omega} \rho_r}{2}} \right] \right) \rho$$

at $\tilde{z} = 0$

$$(33) \quad \frac{\partial \rho}{\partial \tilde{z}} = -\sqrt{\frac{l_h}{a}} i\omega \left(\tilde{\epsilon} + (1-i) \left[(\gamma-1) \sqrt{\frac{\tilde{\omega}}{2}} + \frac{\tilde{k}_r^2}{\tilde{\omega}^2} \sqrt{\frac{\tilde{\omega} \rho_r}{2}} \right] \right) \rho$$

at $\tilde{z} = \frac{L}{a}$.

The boundary conditions couple the different modes of vibration together. The eigenvalues for the radial modes appear in the longitudinal boundary conditions, while the longitudinal and azimuthal eigenvalues appear in the radial boundary conditions. One can resolve this coupling problem by using the zeroth order approximation to the radial eigenvalues, which comes from the $\frac{\partial \rho_r}{\partial r} = 0$ condition, in the longitudinal boundary conditions and vice versa. This works because, while the modified boundary conditions produce a change of order $\sqrt{l_h/a}$ in the zeroth order eigenvalues, this in turn produces a change of only order l_h/a in the other boundary conditions.

Chapter 4: EIGENVALUES

The modified boundary conditions (equations 31,32,33) can be applied to the nonhomogeneous wave equation in cylindrical coordinates which governs the propagational mode.

$$\left(\nabla^2 - \frac{1}{c^2} \frac{\partial^2}{\partial t^2} \right) p = F(r, t)$$

While the forcing function $F(r, t)$ is arbitrary for the purpose of finding $Q(\omega)$, it is commonly expressed in photo-acoustic spectroscopy literature as $-\frac{(\alpha-1)}{c^2} \frac{\partial \bar{Q}}{\partial t}$, where \bar{Q} is the net rate of energy release into the thermal mode.⁶

$$(34) \quad \left(\nabla^2 - \frac{1}{c^2} \frac{\partial^2}{\partial t^2} \right) p = -\frac{(\alpha-1)}{c^2} \frac{\partial \bar{Q}}{\partial t}$$

One begins by solving the homogeneous problem for the system eigenfunctions:

$$(35) \quad \nabla^2 p + \tilde{k}^2 p = 0 \quad \tilde{k}^2 = \tilde{k}_r^2 + \tilde{k}_z^2$$

The azimuthal solution is

$$\Theta_m = a_m \cos m\theta + b_m \sin m\theta$$

The condition $\Theta_m(0) = \Theta_m(2\pi)$ implies that m is an integer. The radial solution R is a linear combination of Bessel's functions $J_m(\tilde{k}_r \tilde{r})$ and $N_m(\tilde{k}_r \tilde{r})$. The coefficient of the $N_m(\tilde{k}_r \tilde{r})$ term must equal zero since the problem must have finite solutions in the bounded region, and $N_m(\tilde{k}_r \tilde{r})$ is singular at $\tilde{r} = 0$.

$$R_{mn} = c_{mn} J_m(\tilde{k}_r \tilde{r})$$

The eigenvalues will be just a small perturbation of order $\sqrt{1_h}/a$ from the rigid, nonviscous, nonconductive eigenvalues.

$$(36) \quad \tilde{k}_r = \tilde{k}_{r_0} + \sqrt{\frac{1_h}{a}} \xi_r$$

where for $m = 0$

$$\tilde{k}_{r_0} = 0.000, 3.832, 7.016, \dots$$

for $m = 1$

$$\tilde{k}_{r_0} = 1.842, 5.332, 8.536, \dots$$

for $m = 2$

$$\tilde{k}_{r_0} = 3.054, 6.706, 9.970, \dots$$

for $m = 3$

$$\tilde{k}_{r_0} = 4.201, 8.015, \dots$$

etc.

These values of \tilde{k}_{r_0} appear in the longitudinal boundary condition at $\tilde{z} = 0$ and $\tilde{z} = \frac{L}{a}$.

The longitudinal eigenvalue \tilde{k}_z and the corresponding eigenfunction Z are small perturbations from the $\frac{\partial Z}{\partial n} = 0$ boundary condition values.

$$(37) \quad Z = \cos \left(\left[\tilde{k}_{z_0} + \eta_z \sqrt{\frac{k_n}{a}} \right] \tilde{z} + \delta_z \sqrt{\frac{k_n}{a}} \right)$$

$$\tilde{k}_{z_0} = \frac{p\pi a}{L}, \text{ where } p \text{ is an integer}$$

Applying the boundary condition, the values of η_z and δ_z to first order in $\sqrt{k_n}/a$ are

$$(38a) \quad \eta_z = \frac{2 B_1(\tilde{\omega}_0)}{\tilde{k}_{z_0} \frac{L}{a}}$$

$$(38b) \quad \delta_z = \frac{-B_1(\tilde{\omega}_0)}{\tilde{k}_{z_0}}$$

where, $B_1(\tilde{\omega}_0) = \tilde{\omega}_0 \left(\tilde{\epsilon} + (1-\tilde{\epsilon}) \left[(\tilde{\omega}_0)^2 \frac{1}{2} + \frac{\tilde{k}_{r_0}^2}{\tilde{\omega}_0^2} \sqrt{\frac{\tilde{\omega}_0 P_r}{2}} \right] \right)$.

Both η_z and δ_z are undefined for $\tilde{k}_{z_0} = 0$. The solutions for $\tilde{k}_{z_0} = 0$ are

$$(39a) \quad \eta_2^0 = \left(\frac{2 B_1(\tilde{\omega}_0)}{\frac{L}{a} \sqrt{\frac{k_n}{a}}} \right)^{1/2}$$

$$(39b) \quad \delta_2^0 = \left(\frac{B_1(\tilde{\omega}_0) \frac{L}{a}}{2 \sqrt{\frac{k_n}{a}}} \right)^{1/2}$$

For $p \neq 0$

$$(40a) \quad Z_{mnp} = \cos \left(\left[\frac{p\pi a}{L} + \frac{\sqrt{\frac{k_n}{a}} 2 B_1(\tilde{\omega}_0)}{p\pi} \right] \tilde{z} + \frac{\sqrt{\frac{k_n}{a}} B_1(\tilde{\omega}_0) L}{p\pi a} \right)$$

For $p = 0$

$$(40b) \quad Z_{mn0} = \cos \left(\left[\frac{\sqrt{\frac{k_n}{a}} 2 B_1(\tilde{\omega}_0) a}{L} \right]^{1/2} \tilde{z} + \left[\frac{\sqrt{\frac{k_n}{a}} B_1(\tilde{\omega}_0) L}{2a} \right]^{1/2} \right)$$

The $\tilde{k}_{z_0} = \frac{p\pi a}{L}$ values appear in the radial boundary conditions at $r = a$.

At $\tilde{r} = 1$,

$$\frac{dR}{d\tilde{r}} = -\sqrt{\frac{k_n}{a}} B_2(\tilde{\omega}_0) R$$

where,
$$B_2(\tilde{\omega}_0) = \tilde{\omega}_0 \left(\tilde{\epsilon} + (1-\tilde{\epsilon}) \left[(\tilde{\mu} - 1) \sqrt{\frac{\tilde{\omega}_0}{2}} + \frac{m^2 + \tilde{k}_{z_0}^2}{\tilde{\omega}_0^2} \sqrt{\frac{\tilde{\omega}_0}{2}} P_n \right] \right)$$

By using Taylor series expansions around \tilde{k}_{r_0} to approximate $J_m(\tilde{k}_r \tilde{r})$ and $\frac{dJ}{d(k_r \tilde{r})}$ at $k_{r_0} + \tilde{\zeta}_r \sqrt{\frac{k_n}{a}}$, one can show that

$$(41a) \quad \tilde{\zeta}_r = \frac{\tilde{k}_{z_0} B_2(\tilde{\omega}_0)}{(\tilde{k}_{z_0}^2 - m^2)}$$

This is undefined for $\tilde{k}_{z_0}^2 = m^2$ which occurs only at $\tilde{k}_{z_0} = m = 0$.

For $\tilde{k}_{z_0} = m = 0$

$$(41b) \quad \tilde{\zeta}_r^0 = \left[\frac{2 B_2(\tilde{\omega}_0)}{\sqrt{\frac{k_n}{a}}} \right]^{1/2}$$

For $\tilde{k}_{r_0} \neq 0$

$$(42a) \quad R_{mnp} = \sqrt{J_m} \left([L \tilde{k}_{r_0} + \sqrt{\frac{L}{\alpha}} \tilde{k}_{r_0} B_2(\tilde{\omega}_0)] \tilde{r} \right).$$

For $\tilde{k}_{r_0} = 0$

$$(42b) \quad R_{mnp} = \sqrt{J_0} \left([2 \sqrt{\frac{L}{\alpha}} B_2(\tilde{\omega}_0)]^{1/2} \tilde{r} \right).$$

The θ , r , and Z eigenfunctions correspond to azimuthal, radial, and longitudinal standing waves as pictured in Figure 2.

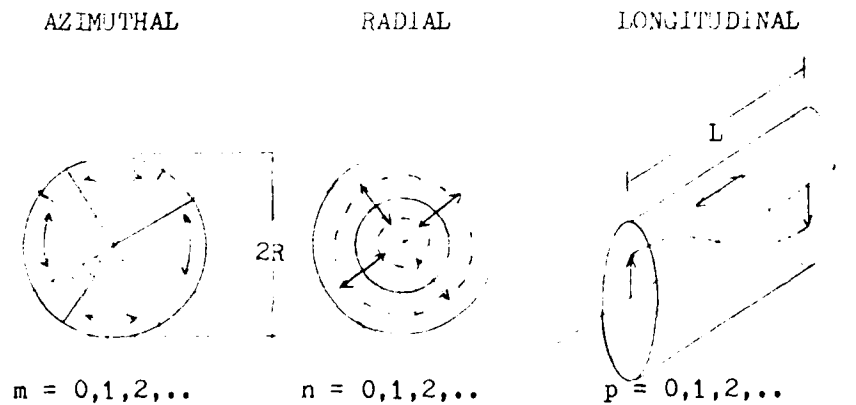


Fig. 2

$$p = \sum_{mnp} A_{mnp} Z_{mnp}(\tilde{z}) R_{mnp}(\tilde{r}) \Theta_m(\theta) e^{-i\tilde{\omega}t}$$

The next step in a complete solution is to express \bar{Q} in terms of the eigenfunctions.

$$\bar{Q} = \sum_{mnp} B_{mnp} Z_{mnp}(\tilde{z}) R_{mnp}(\tilde{r}) \Theta_m(\theta) e^{-i\tilde{\omega}t}$$

However, that requires knowledge of the absorption characteristics of the gas, and is not within the scope of this paper. One can get some very important information about the shape of the resonant peaks, and the phase shifts through resonance without knowing B_{mnp} .

$$(43) \quad \frac{p}{Q} = \frac{A_{mnp}}{B_{mnp}} = \frac{-i(\mathcal{H}-1)\tilde{\omega}}{\tilde{\omega}^2 - (\tilde{k}_r^2 + \tilde{k}_z^2)}$$

System resonances occur at $\tilde{\omega}^2 = \text{Re}(k_r^2 + k_z^2)$, while the finite imaginary values of $\tilde{\zeta}_r$ and $\tilde{\eta}_z$ keep the resonant peaks from being infinite. One measure of the sharpness of a resonance peak is the $Q(\omega)$ at resonance. The acoustic $Q(\omega)$ is the resonant frequency divided by the peak width at the half-power point. For a system excited by a single laser pulse the rate of signal decay depends on the magnitude of the system dissipation. $Q(\omega) = 2/\delta$ where δ is the logarithmic decrement or fractional amplitude loss per radian of the signal. The acoustic signal amplification due to resonance reported by Dewey et. al. is proportional to $Q(\omega)$.^{2,9}

One can look at A_{mnp}/B_{mnp} near resonance by defining ω_0 as the zeroth order resonant frequency plus a small perturbation of order $\sqrt{1_h/a}$.

$$(44) \quad \tilde{\omega} = \tilde{\omega}_0 + \Omega \sqrt{\frac{k_h}{a}} \quad \tilde{\omega}_0^2 = \tilde{k}_{r_0}^2 + \tilde{k}_{z_0}^2$$

For $\tilde{k}_{r_0} \neq 0, \tilde{k}_{z_0} \neq 0$

$$(45) \quad \frac{A_{mnp}}{B_{mnp}} = \frac{-i(\mathcal{H}-1)(\tilde{\omega}_0 + \Omega \sqrt{\frac{k_h}{a}})}{(\tilde{\omega}_0^2 + 2\Omega \tilde{\omega}_0 \sqrt{\frac{k_h}{a}}) - [(\tilde{k}_{r_0}^2 + 2\sqrt{\frac{k_h}{a}} \tilde{k}_{r_0} \tilde{k}_{z_0} - m^2) - (\tilde{k}_{z_0}^2 + 4\sqrt{\frac{k_h}{a}} \tilde{k}_{z_0} \tilde{k}_{r_0})]}$$

In most photo-acoustic cells the walls are sufficiently rigid to assume $\tilde{\zeta} \ll 0(1_h/a)$. In such a case

$$(46) \quad \frac{A_{mnp}}{B_{mnp}} = \frac{-i(\mathcal{H}-1)(\tilde{\omega}_0 + \Omega \sqrt{\frac{k_h}{a}})}{2\Omega \tilde{\omega}_0 \sqrt{\frac{k_h}{a}} - 2(1+i)\sqrt{\frac{k_h}{a}} \tilde{\omega}_0^{3/2} D}$$

where

$$D = \left(\frac{k_{r_0}}{k_{r_0}^2 - m^2} \left[\frac{(\mathcal{H}-1)}{\sqrt{2}} + \frac{m^2 \sqrt{k_{r_0}}}{\tilde{\omega}_0^2 \sqrt{2}} \sqrt{P_1} \right] + \frac{2\alpha}{L} \left[\frac{(\mathcal{H}-1)}{\sqrt{2}} + \frac{\tilde{k}_{z_0}^2}{\tilde{\omega}_0^2} \sqrt{P_1} \right] \right)$$

Viscosity and thermal conductivity shift the cylinder resonances to higher frequencies. The resonant peak occurs at

$$(47) \quad \tilde{\omega}_{res} = \tilde{\omega}_0 + \sqrt{\frac{l_h}{a}} \tilde{\omega}_0^{1/2} D.$$

To find $Q(\omega)$ one needs to solve for $\Omega_{1/2}$ where $|A_{mnp}/B_{mnp}| = 1/\sqrt{2} |A_{mnp}/B_{mnp}|_{res}$. To first order in l_h/a the resonant peak is a parabola and

$$(48) \quad \Omega_{1/2} = \tilde{\omega}_0^{1/2} D \pm \tilde{\omega}_0^{1/2} D.$$

Therefore the width at the half-power point is $2\tilde{\omega}_0^{1/2}D$, and the formula for $Q(\omega)$ is

$$(49) \quad Q(\omega) = \frac{\omega_{res}}{\Delta\omega_{1/2 power}} \approx \frac{\tilde{\omega}_0}{2\sqrt{\frac{l_h}{a}} \tilde{\omega}_0^{1/2} D}$$

The phase angle as one passes through resonance is equal to the arc-tangent of the imaginary part of A_{mnp}/B_{mnp} divided by the real part. The solution for the phase angle ϕ is

$$(50) \quad \phi = \tan^{-1} \left[\frac{\tilde{\omega}^2 - \tilde{\omega}_0^2 - 2\sqrt{\frac{l_h}{a}} \tilde{\omega}_0^{1/2} D}{-2\sqrt{\frac{l_h}{a}} \tilde{\omega}_0^{1/2} D} \right]$$

For the special cases when either $\tilde{k}_{r_0} = 0$ or $\tilde{k}_{z_0} = 0$ only the formula for D changes.

For $\tilde{k}_{r_0} \neq 0, \tilde{k}_{z_0} = 0$

(51)

$$D = \frac{1}{\sqrt{2}} \left[\frac{\tilde{k}_{r_0}^2}{\tilde{k}_{r_0}^2 m^2} \left((\beta^2 - 1) + \frac{m^2}{\tilde{\omega}_0^2} \sqrt{P_1} \right) + \frac{a}{L} \left((\beta^2 - 1) + \sqrt{P_1} \right) \right]$$

For $k_{r_0} = 0$, $k_{z_0} \neq 0$

$$(52) \quad D = \frac{1}{\sqrt{2}} \left[((\gamma^2 - 1) + \sqrt{\rho_r}) + \frac{2a}{L} (\gamma^2 - 1) \right]$$

Some literature sources refer to an acoustic $Q(\omega)$ which is measured at the half-amplitude rather than half-power point of the signal. The formula for the half-amplitude $Q(\omega)$ differs from the half-power $Q(\omega)$ by a factor of $1/\sqrt{3}$.

Another formula for $Q(\omega)$ developed from Morse and Ingard¹¹ for the $m = 0$, $\tilde{k}_{z_0} = 0$ radial modes is common in the photo-acoustic literature.^{3,12}

$$(53) \quad Q(\omega) = \frac{L}{d_v + (\gamma^2 - 1) d_h \left(1 + \frac{L}{a}\right)}$$

This formula is usually adequate, since the first radial mode is the most strongly excited by the usual beam, cylinder configuration. When equation 49 is put into the same form as 53 for easy comparison the results are

$$(54) \quad Q(\tilde{\omega}) = \frac{L}{d_v \left(\frac{(2 - \delta_{0,z}) \tilde{k}_{r_0}^2}{\tilde{k}_{r_0}^2 + \tilde{k}_{z_0}^2} + \frac{L \tilde{k}_{r_0}^2 (\tilde{k}_{z_0}^2 + m^2)}{a (\tilde{k}_{r_0}^2 - m^2) (\tilde{k}_{r_0}^2 + \tilde{k}_{z_0}^2)} \right) + (\gamma^2 - 1) d_h \left(2 - \delta_{0,z} + \frac{L}{a} \frac{\tilde{k}_{r_0}^2}{(\tilde{k}_{r_0}^2 - m^2)} \right)}$$

$$\delta_{0,z} = \begin{cases} 0 & \text{for } \tilde{k}_{z_0} \neq 0 \\ 1 & \text{for } \tilde{k}_{z_0} = 0 \end{cases} \quad d_v = \sqrt{\frac{2\mu}{\rho\omega}} \quad d_h = \sqrt{\frac{2K}{\rho\omega C_p}}$$

$$\tilde{k}_{z_0} = \frac{\rho \pi a}{L}$$

\tilde{k}_{r_0} = the roots of the first derivative of the m^{th} order Bessel's function

Equation 54 reduces to 53 for $m = \tilde{k}_{z_0} = 0$.

Equation 54 is more general because it is valid for all the system resonances. Current research requires this additional flexibility. For example, some multipass configurations which bounce the laser beam back and forth inside the cell to increase the effective absorption cross section may not excite the first radial mode optimally. Angus, Marinero, and Colles observed the spectrum of NO_2 operating in a small diameter cell at the first longitudinal resonance.¹⁸ They achieved an amplification factor of 50 without suffering from losses due to a larger cell. Koch and Lahmann detected small levels of sulphur dioxide in air using a first longitudinal resonance.¹⁶

Chapter 5: EXPERIMENT

To test the applicability of the results presented in the first half of this paper, we devised an experiment to measure the values of $Q(\omega)$ and phase shift through the acoustic resonances of a cylinder.

Figure 3 summarizes the experimental set up.

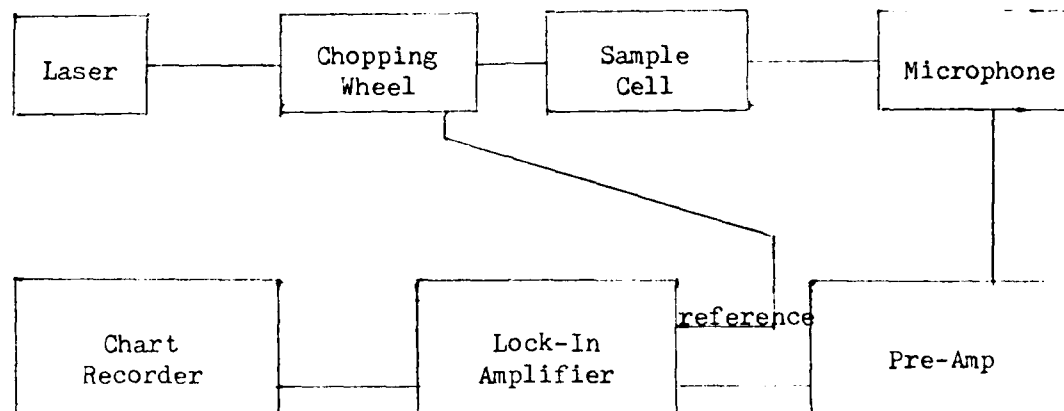


Fig. 3

A visible laser light beam was passed through a rotating chopper wheel, and then through the sample cell. The resulting pressure pulses were detected by a microphone. The signal from the microphone was amplified and transmitted to a lock-in amplifier. The signal was synchronously detected by the lock-in amplifier which was referenced to the chopping frequency. During the experiment the chopping frequency was steadily increased, and the magnitude and phase outputs of the lock-in amplifier were plotted on the chart recorder as a function of frequency. The linearity of this system was previously tested, and it is assumed that the signal plotted was proportional to the pressure changes in the cell.

We conducted our experiments primarily at atmospheric pressure, and room temperature. We filled our cell with dry air and nitric oxide. Before each experiment the cell was pumped out overnight with a vacuum pump. We filled the cell with 1 to 3 Torr of NO, monitoring its pressure on a Bourdon Gauge. Then we filled the cell to one atmosphere with dry air by passing room air slowly through a liquid nitrogen trap to condense out all water vapor. Upon contact with air, NO reacts to form NO₂ which is brown in color, and a strong absorber of visible light. Figure 4 shows the absorption spectrum of NO₂¹⁷, and the locations of the output lines from the Spectra Physics model 171 Argon/Krypton laser.

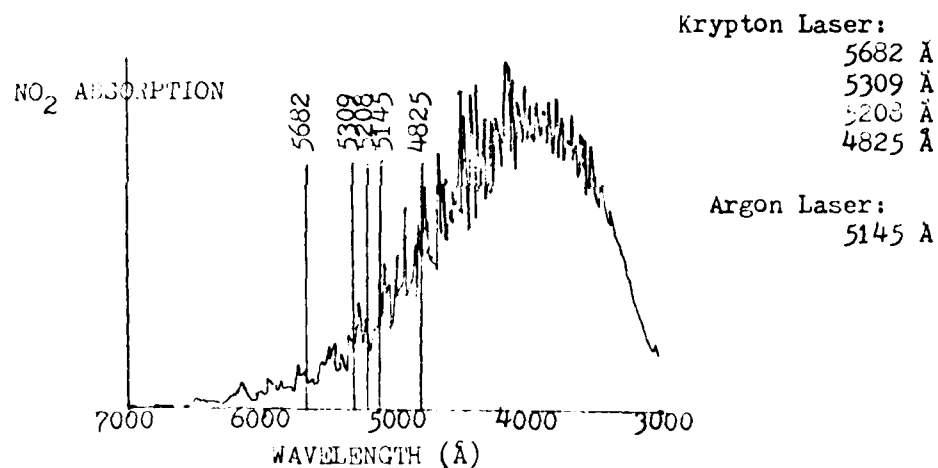


Fig. 4

We used both the Argon and Krypton laser tubes during different parts of the experiment. The difference in wavelengths between the two lasers made no difference in the experiment, since we were concerned only with creating enough signal to measure $Q(\omega)$, and not in the absorption mechanisms.

We mounted a Bruel and Kjaer microphone (sensitivity = $4.95/\text{dyne}/\text{cm}^2$)

midway along the axis, flush with the side wall of the cell. A ramp voltage applied to the chopper wheel controller increased the chopping frequency linearly during each run.

We used an existing acoustic cell ($a = 5.207\text{cm}$. $L = 9.2075\text{cm}$.) with large glass windows entirely covering the ends of the cell. See Figure 5.

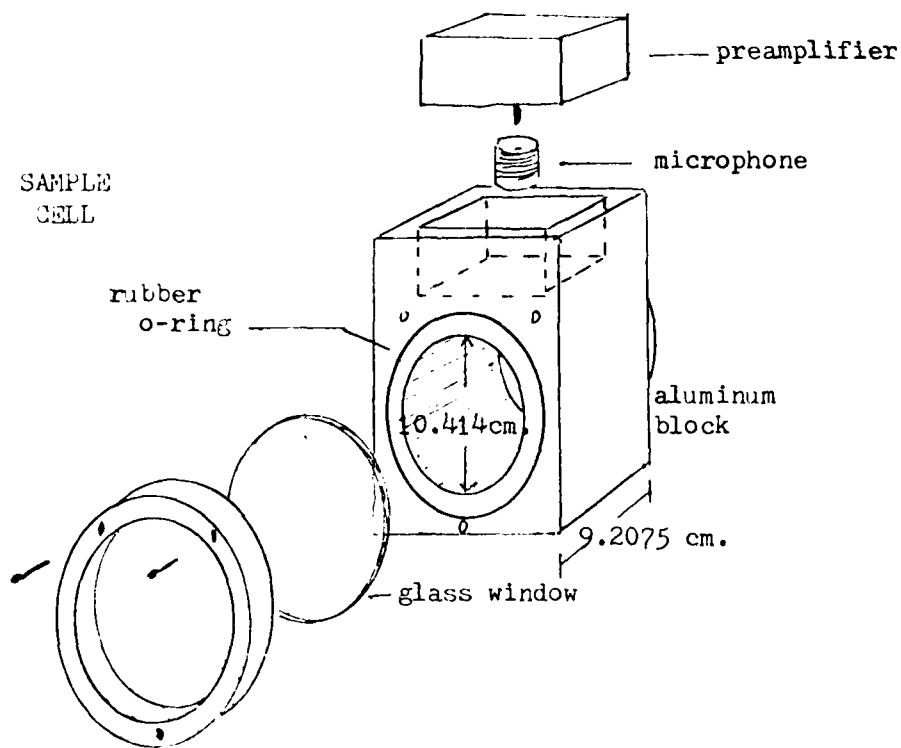


Fig. 5

Such a configuration made it difficult to distinguish between window absorption and gas absorption signals, but again we were concerned only with having enough signal, and not in where the signal came from. The large windows enabled us to move the laser beam around within the cell to variously excite and suppress different modes. Specifically, an off center beam could excite the azimuthal modes which were not excited by a

centered beam. Shining the beam through the cell at $r = .63a$ suppressed the first radial mode, since $r = .63a$ corresponds to the first zero of the J_0 Bessel's function.

In calculating the expected $Q(\omega)$ s for the various resonances we assume that the concentration of NO_2 (<.5%) was so small that the dry air used as a buffer gas determined the cell acoustics and dissipative parameters. Table 1 lists the necessary physical constants for air at one atmosphere from the Chemical Rubber Company Handbook of Chemistry and Physics.

Table 1

	$\gamma^A = 1.40$	$C_p = .241$		
Temperature ($^{\circ}\text{C}$)	18.3	21.1	23.9	26.7
c (m/s)	342.2	344.0	345.6	347.3
ρ (gm/lt)	1.212	1.200	1.189	1.178
κ (cal/gm cm^2 ($^{\circ}\text{C}/\text{cm}$) 10^{-6})	60.81	61.27	61.74	62.20
μ (micropoises)	182.0	184.2	185.5	186.6
$\sqrt{\text{Pr}}$.8514	.8512	.8509	.8503
$\sqrt{1_h/a}$	1.081×10^{-3}	1.088×10^{-3}	1.094×10^{-3}	1.101×10^{-3}

Appendix A lists the mode shapes and frequencies of the 30 lowest natural frequencies.

We did not observe all of the resonances listed in Appendix A. Many were only weakly excited, or buried under the strong signal of a nearby resonance. The odd harmonics of the longitudinal modes were especially difficult to detect. They were excited by the attenuation of laser power as it passed through the absorbing gas. Even with a strong absorber like NO_2 the odd longitudinal harmonics were much weaker than the radial sig-

nals. The location of the microphone at the midway point along the axis, a node of the odd longitudinal harmonics, made detecting them even more difficult.

The calculated and measured values of $Q(\omega)$ for the observed resonances at one atmosphere are in Table 2.

Table 2

Mode	Q_{calc}	Q_{meas}	Q_{meas}/Q_{calc}
(1,0,0)	533.1	383.4	.719
(2,0,0)	549.2	363.3	.661
(0,1,0)	1135	572.1	.504
(0,2,0)	1543	438.6	.284
(0,0,1)	503.8	412.1	.818
(0,0,2)	714.2	577.4	.808
(1,1,0)	1279	567.6	.474

The signal to noise ratio for this experiment is probably on the order of 100:1, and should not cause any error in measuring $Q(\omega)$. However, there may be some error in the measuring of $Q(\omega)$ due to uncertainty in fixing the base line of a peak from which we determine its half maximum. This is because so many of the peaks overlapped with peaks of other resonances. Graphs of the phase and amplitude versus frequency for each resonance are in Appendix B.

CONCLUSIONS

The results for the longitudinal modes were quite close to their predicted values, while the azimuthal and radial modes were not. Some possible sources of the discrepancy are:

1. Rough Surfaces - With boundary layer thicknesses on the order of 10^{-3} cm., slight surface roughness could have seriously affected the results.

2. Compliant Walls - While the cell was bored from a heavy block of aluminum, the glass windows which acted as end walls were thinner and less rigid.

3. The Microphone - The microphone diaphragm was 23.8 mm in diameter, and much less rigid than the cell walls. The mounting of the flat microphone was not flush with the curved walls, which could have significantly altered the cell geometry.

4. Volume Losses - The theory in chapter 2 predicts these losses will be on the order of 10^{-3} times the boundary layer losses.

Rough surfaces would increase viscous losses. The windows were smooth, so we expected to see rough wall losses mostly on modes tangential to the side walls, the longitudinal and azimuthal modes. Since the radial modes suffered the greatest losses beyond those predicted, rough surface losses were probably not the major source of error in this experiment.

Compliant windows would show up as additional acoustic conductance for waves propagating normal to the end walls. These were the longitudinal modes whose $Q(\omega)$ s were very close to their predicted values. Compliant windows were not likely to be the major source of error in this ex-

periment.

Wave reflection off the flat spot on the side wall and the scattering off of the microphone mounting would undoubtedly have the most effect on the radial and azimuthal modes. The radial and azimuthal modes have the largest unexplained losses, so the microphone was probably a major source of experimental error.

One way to verify that the unpredicted losses are due to imprecise cell construction, and not to an error in predicting the fluid mechanical losses is to conduct the experiment at lower pressure. This raises the relative importance of the fluid mechanical losses, without changing the scattering losses, and should result in better agreement between predicted and measured $Q(\omega)$ s.

We measured $Q(\omega)$ for the first radial and first azimuthal modes at one-half atmosphere, and $Q_{\text{meas}}/Q_{\text{calc}}$ improved from .504 to .562, and .719 to .766 respectively. The small improvement was very close to that expected, but still within the bounds of the experimental error. We needed further experiments at 1/4 and 1/8 atmosphere over a wider range of resonances to confirm our hypothesis. However, the laser source broke down before we could take anymore data.

In future experiments one should take great care to make the real cell match the theoretical geometry. Mounting the microphone flush with an end wall may solve the scattering problem. The experiment should cover a wide range of pressures, and possibly use more than one microphone, thus providing access to modes with a node at one microphone.

This paper provides a needed method for predicting the acoustic quality of a given resonant photo-acoustic spectroscopy cell. It presents

a rigorous treatment of the resonant responses of a cylinder to a distributed heat source by showing that one could include viscous, thermal, and compliant boundary losses to first order simply by modifying the boundary conditions on the nondissipative wave equation. The results of the analysis are formulas for $Q(\omega)$ and phase shift through resonance. This paper also presents the results of an experiment conducted to test these formulas. Because of their sensitivity to small changes from the cylindrical geometry, the formulas failed to accurately predict the exact response of the system, but are still useful for comparing the relative advantages of various experimental designs and cell configurations.

APPENDIX A

The Mode Shapes and Frequencies of the 30 Lowest Natural Frequencies
($r = 5.207\text{cm}$, $L = 9.2075\text{cm}$)

m = the azimuthal index
 n = the radial index
 p = the longitudinal index

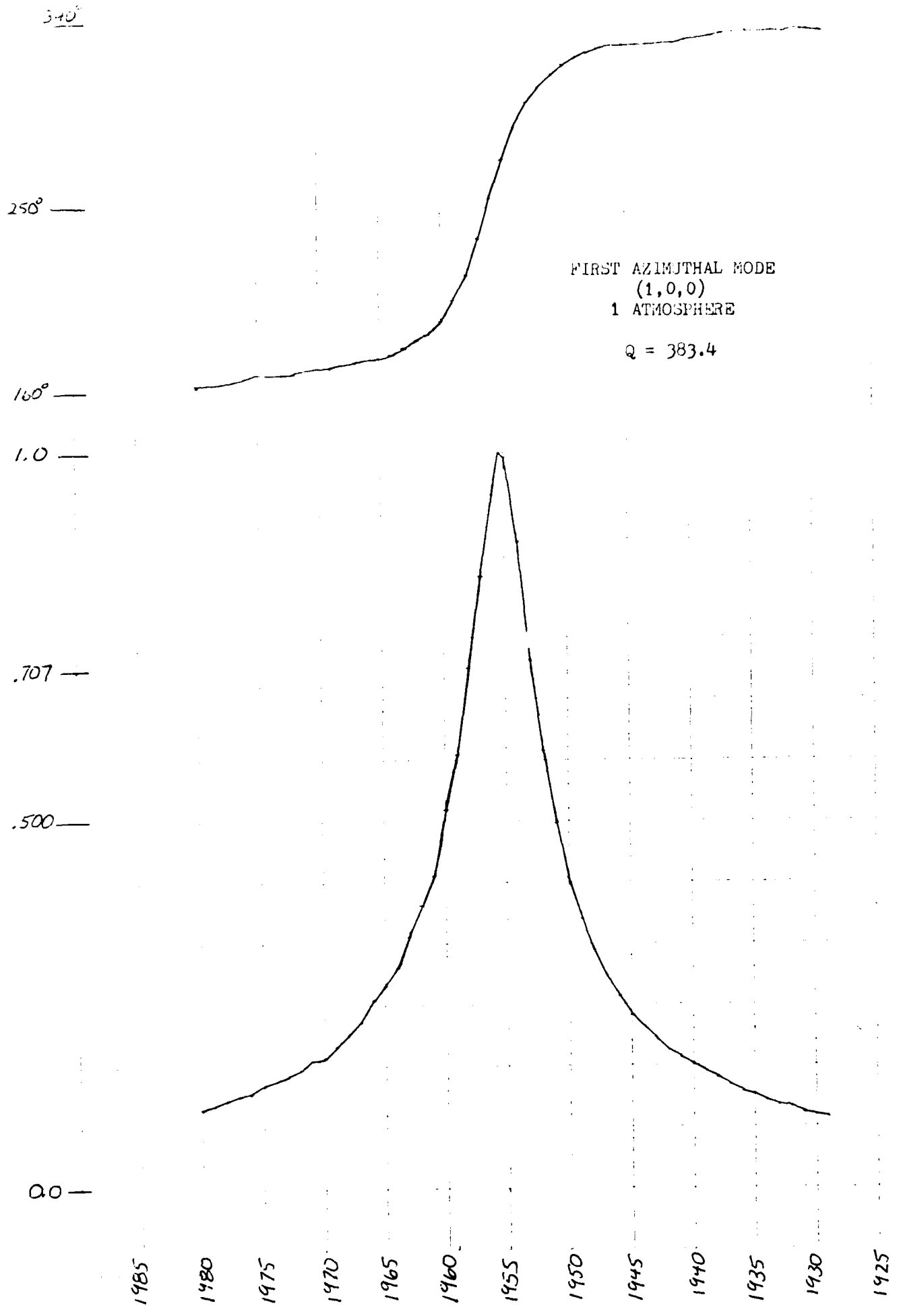
$\tilde{\omega}^2 = (k_r^2 + k_z^2)^{\frac{1}{2}}$	(m,n,p)	f (18.3-26.7 °)
1.777	(0,0,1)	1860 - 1886
1.842	(1,0,0)	1928 - 1955
2.559	(1,0,1)	2678 - 2716
3.054	(2,0,0)	3196 - 3242
3.533	(2,0,1)	3698 - 3750
3.553	(0,0,2)	3718 - 3772
3.832	(0,1,0)	4010 - 4068
4.002	(1,0,2)	4188 - 4248
4.201	(3,0,0)	4397 - 4460
4.224	(0,1,1)	4421 - 4484
4.561	(3,0,1)	4773 - 4842
4.685	(2,0,2)	4903 - 4973
5.226	(0,1,2)	5469 - 5548
5.317	(4,0,0)	5565 - 5644
5.330	(0,0,3)	5578 - 5658
5.332	(1,1,0)	5580 - 5660
5.502	(3,0,2)	5758 - 5841
5.606	(4,0,1)	5867 - 5951
5.639	(1,0,3)	5902 - 5986
6.143	(2,0,3)	6429 - 6521
6.395	(4,0,2)	6693 - 6789
6.407	(1,1,2)	6705 - 6801
6.416	(5,0,0)	6715 - 6811
6.564	(0,1,3)	6870 - 6968
6.658	(5,0,1)	6968 - 7068
6.706	(2,1,0)	7018 - 7119
6.786	(3,0,3)	7102 - 7204
6.937	(2,1,1)	7260 - 7364
7.016	(0,2,0)	7343 - 7448
7.106	(0,0,4)	7437 - 7543

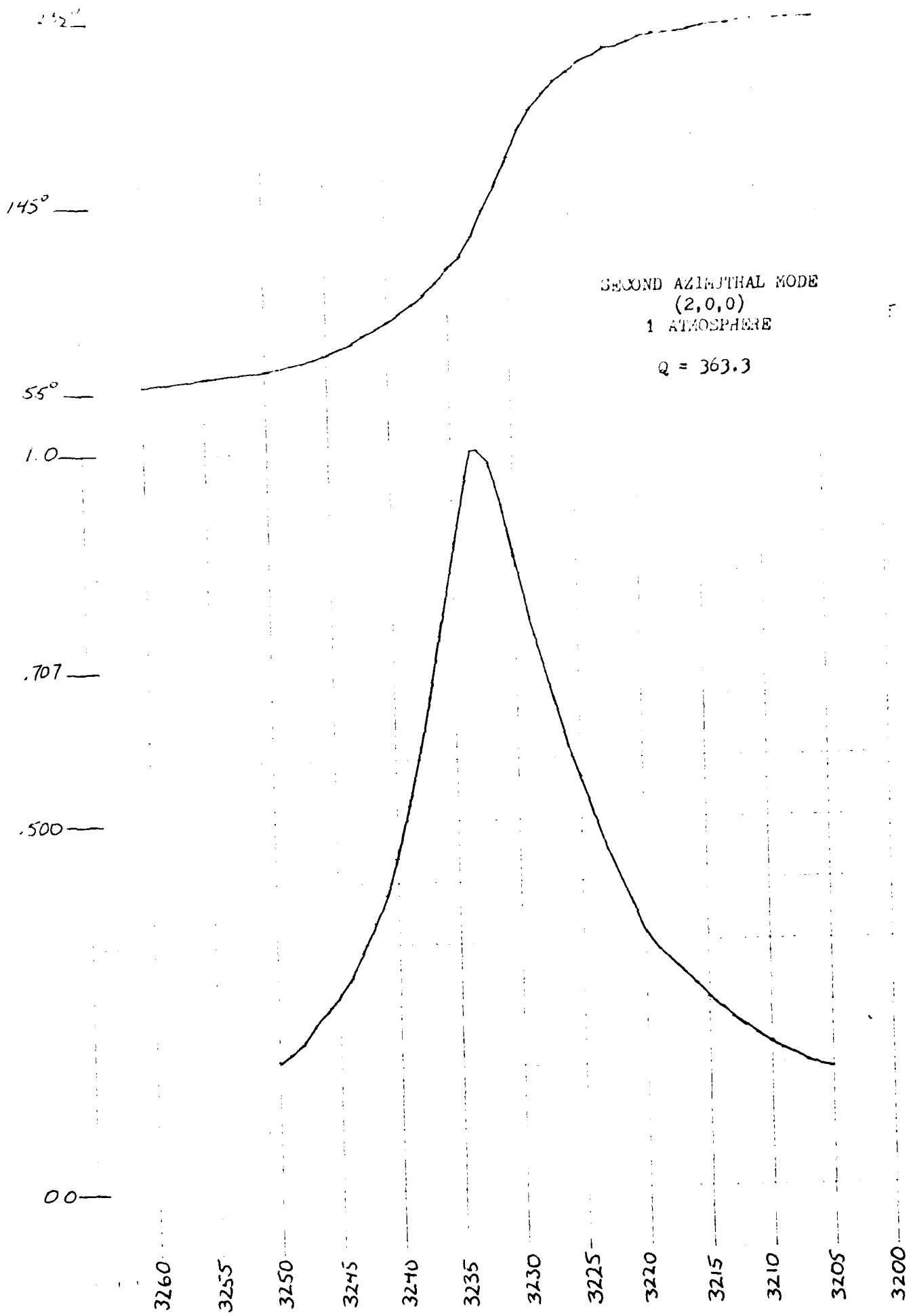
APPENDIX B

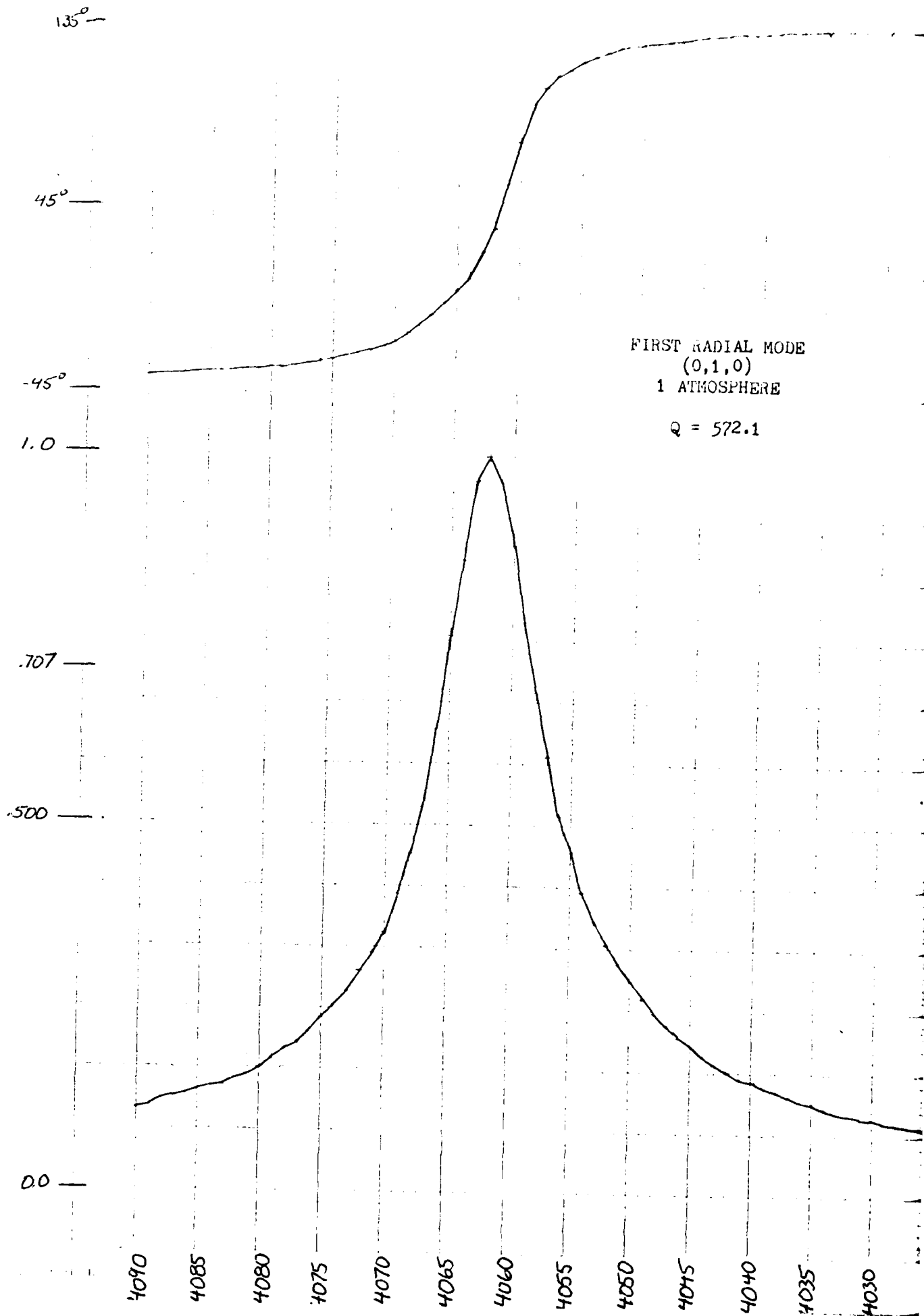
GRAPHS OF PHASE AND AMPLITUDE
VERSUS FREQUENCY FOR MEASURED RESONANCES

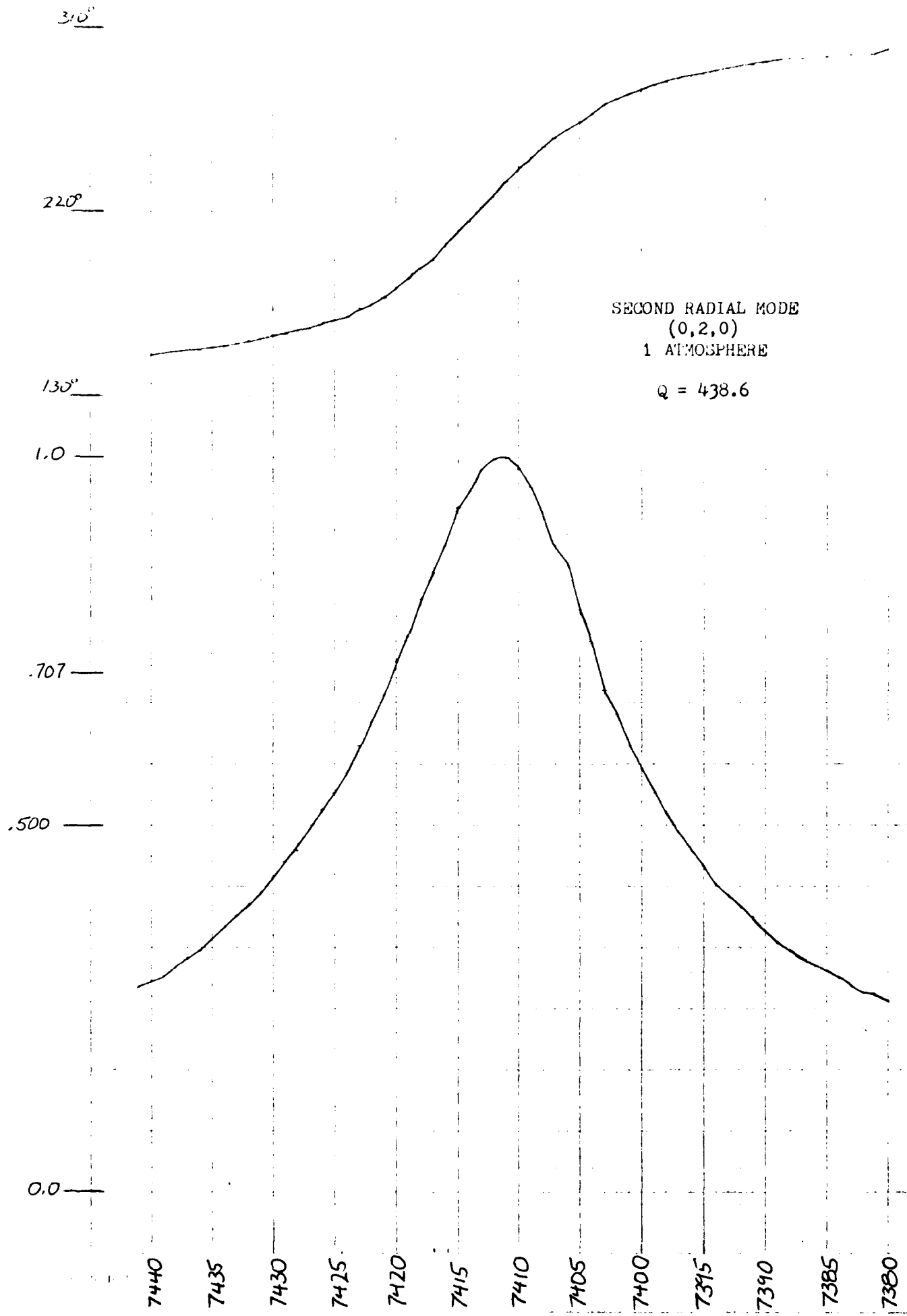
The amplitudes of all the peaks are normalized to one.

The frequency is given in Hz.



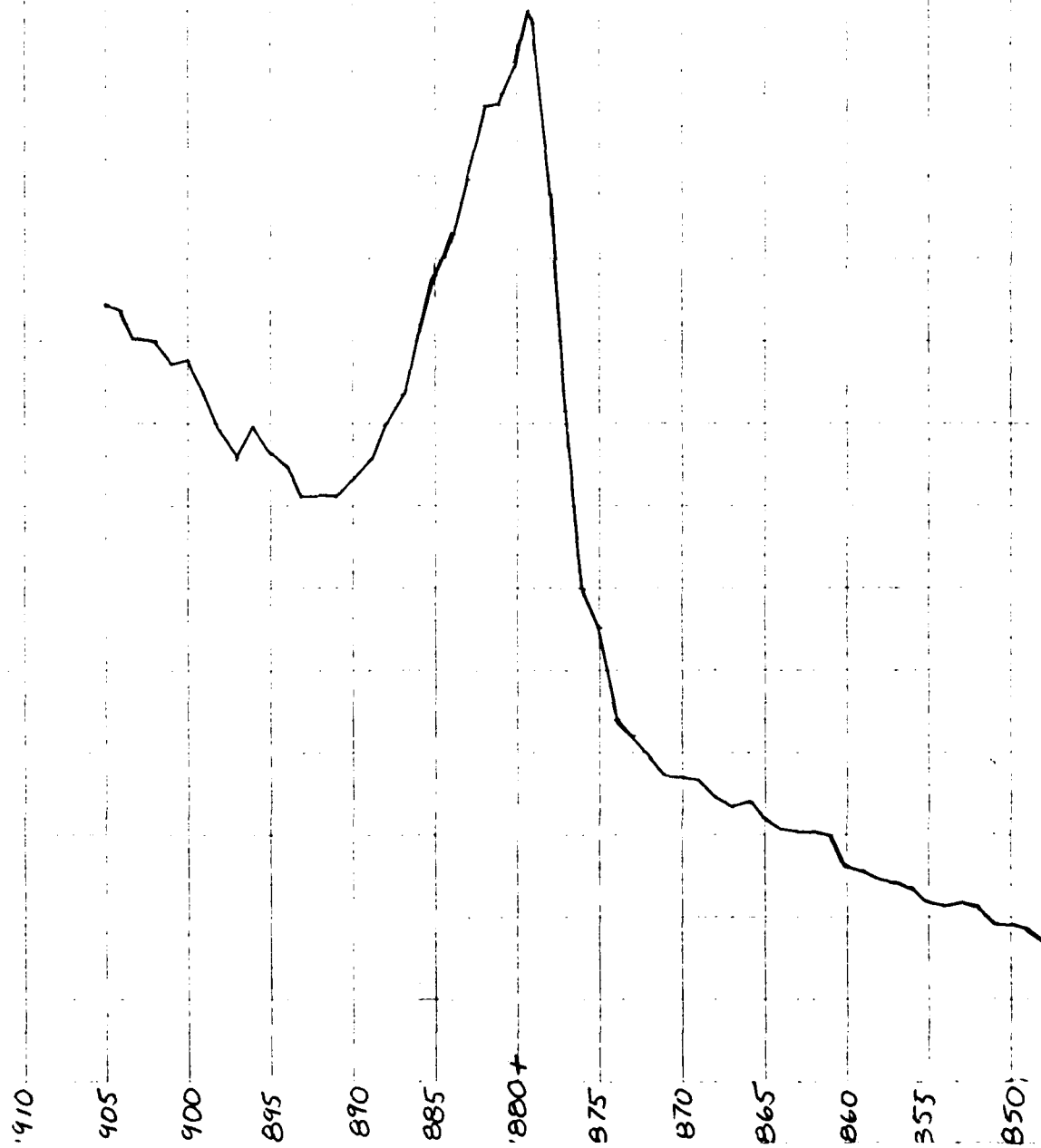






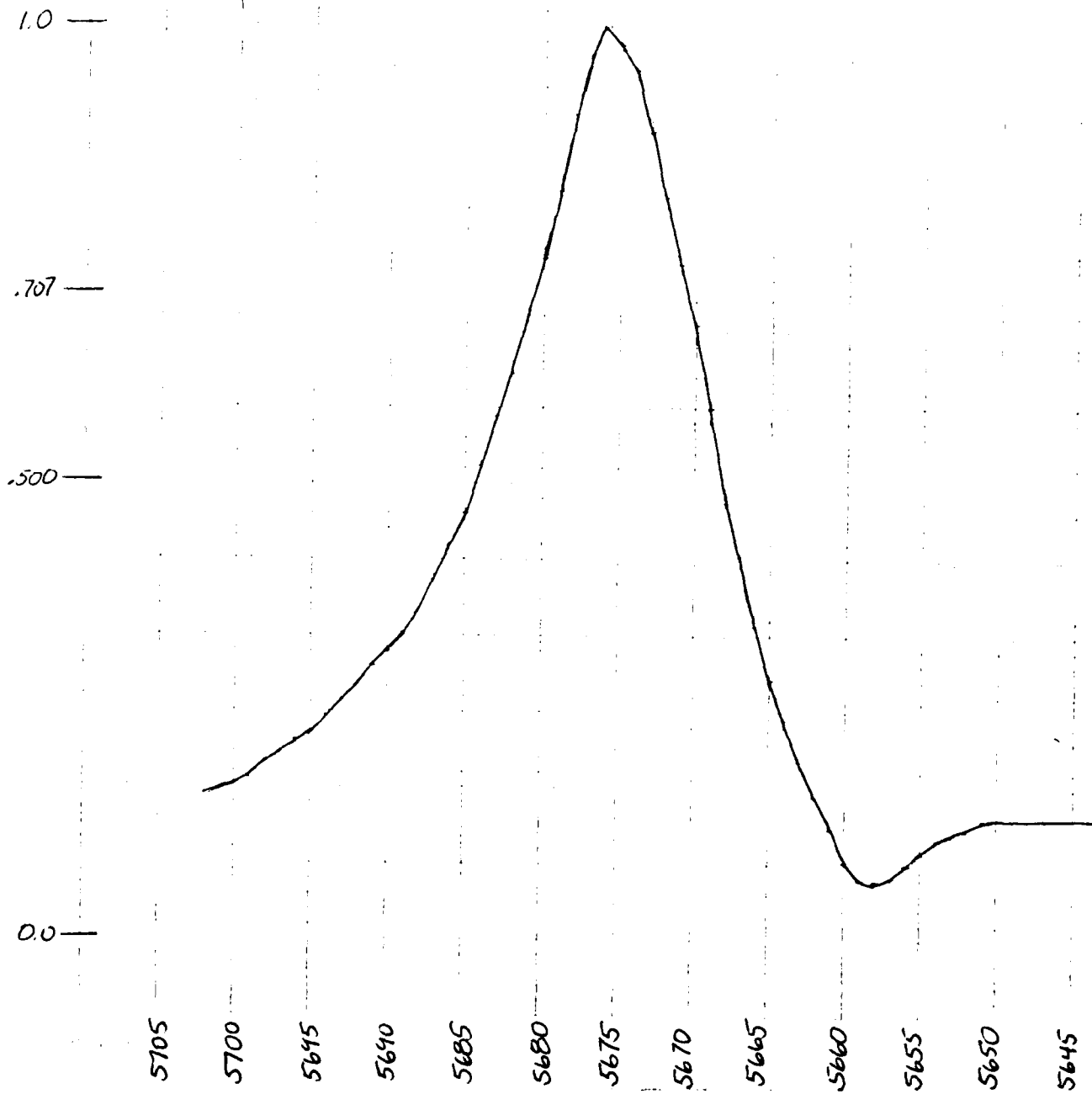
FIRST LONGITUDINAL MODE
(0,0,1)
1 ATMOSPHERE

Q = 412.1



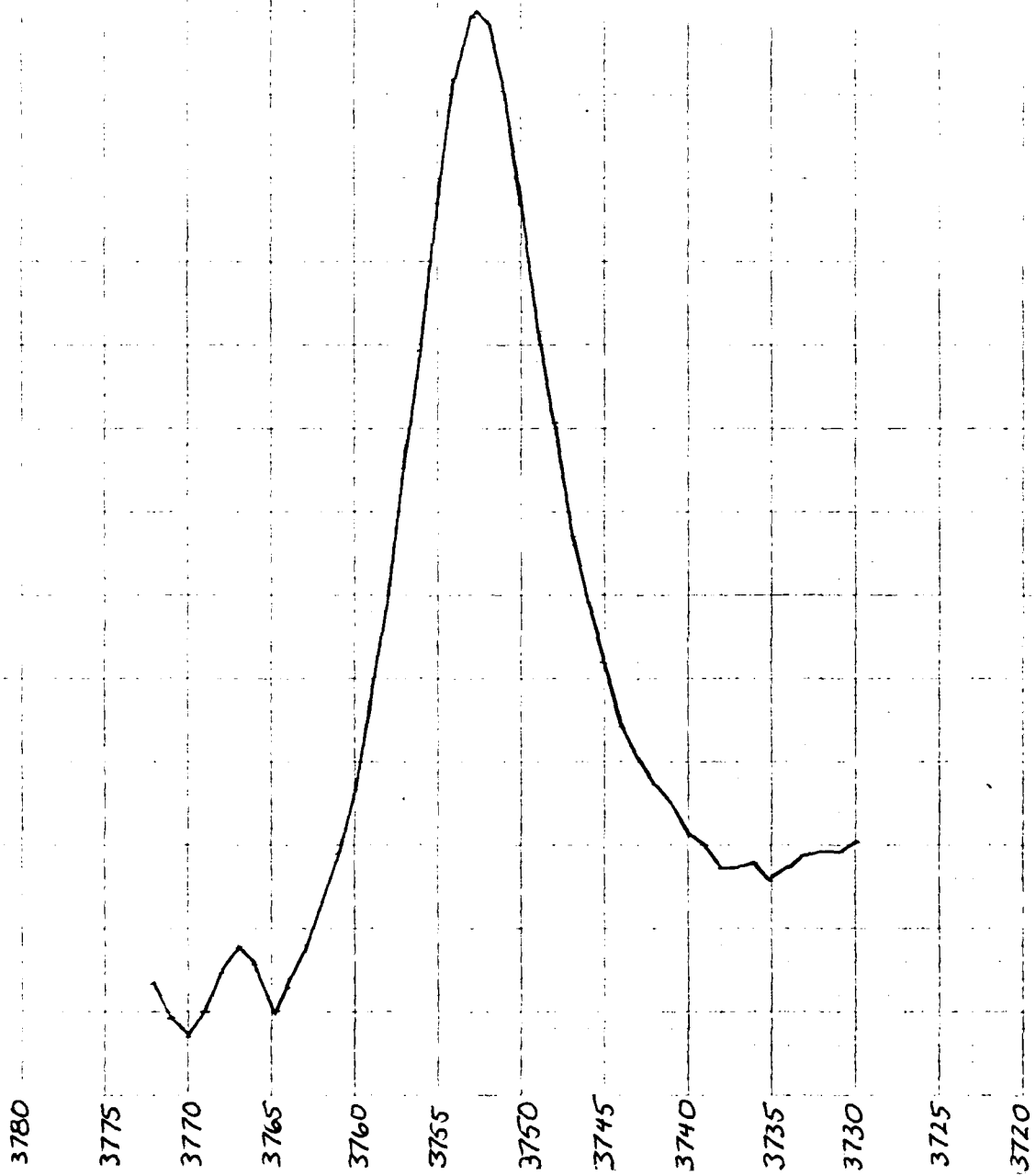
RADIAL-AZIMUTHAL COUPLED MODE
(1,1,0)
1 ATMOSPHERE

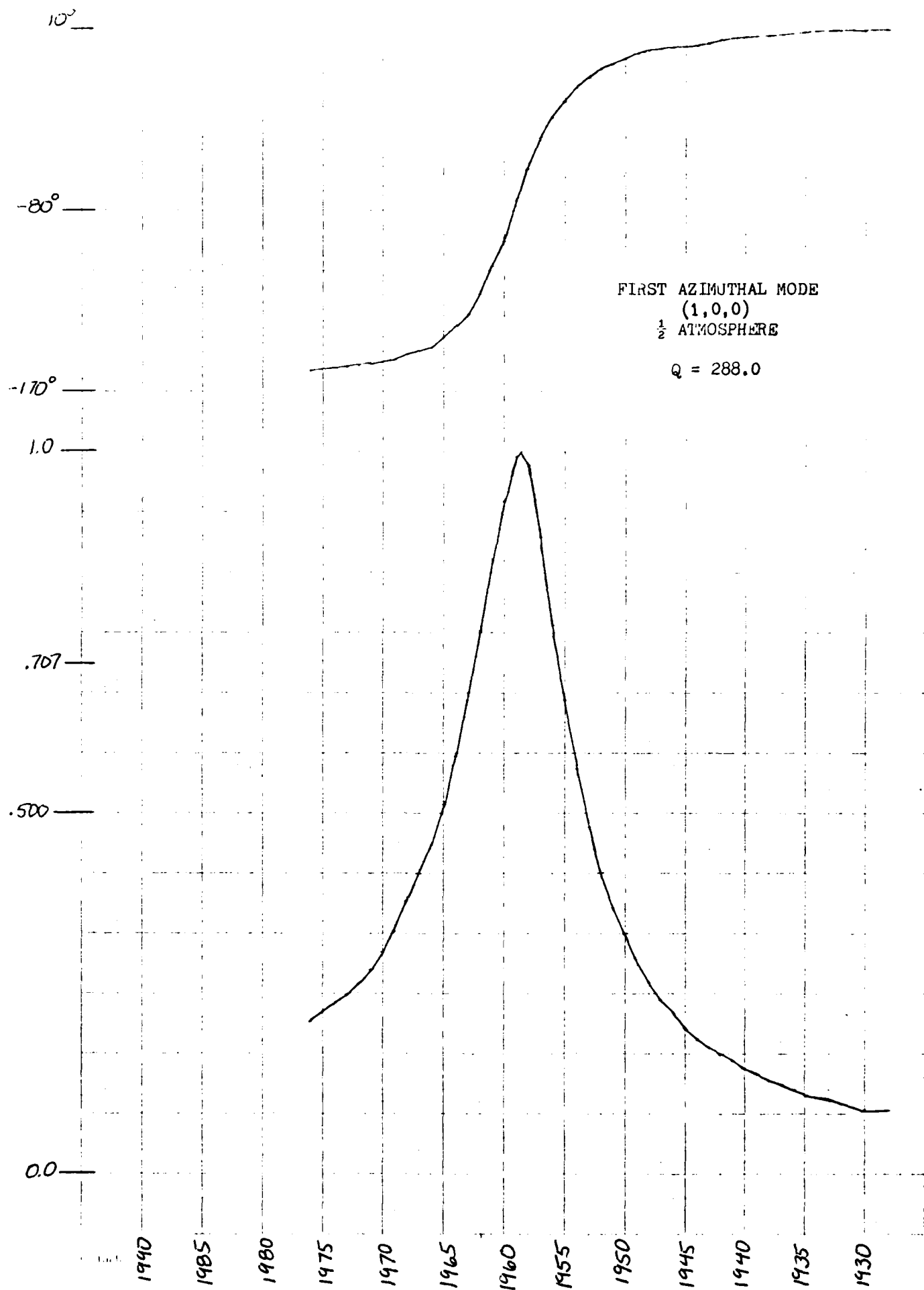
$Q = 567.6$



SECOND LONGITUDINAL MODE
(0,0,2)
1 ATMOSPHERE

Q = 577.4





FIRST RADIAL MODE
(0,1,0)
 $\frac{1}{2}$ ATMOSPHERE

Q = 448.3

1.0

.707

.500

0.0

4110

4105

4100

4095

4090

4085

4080

4075

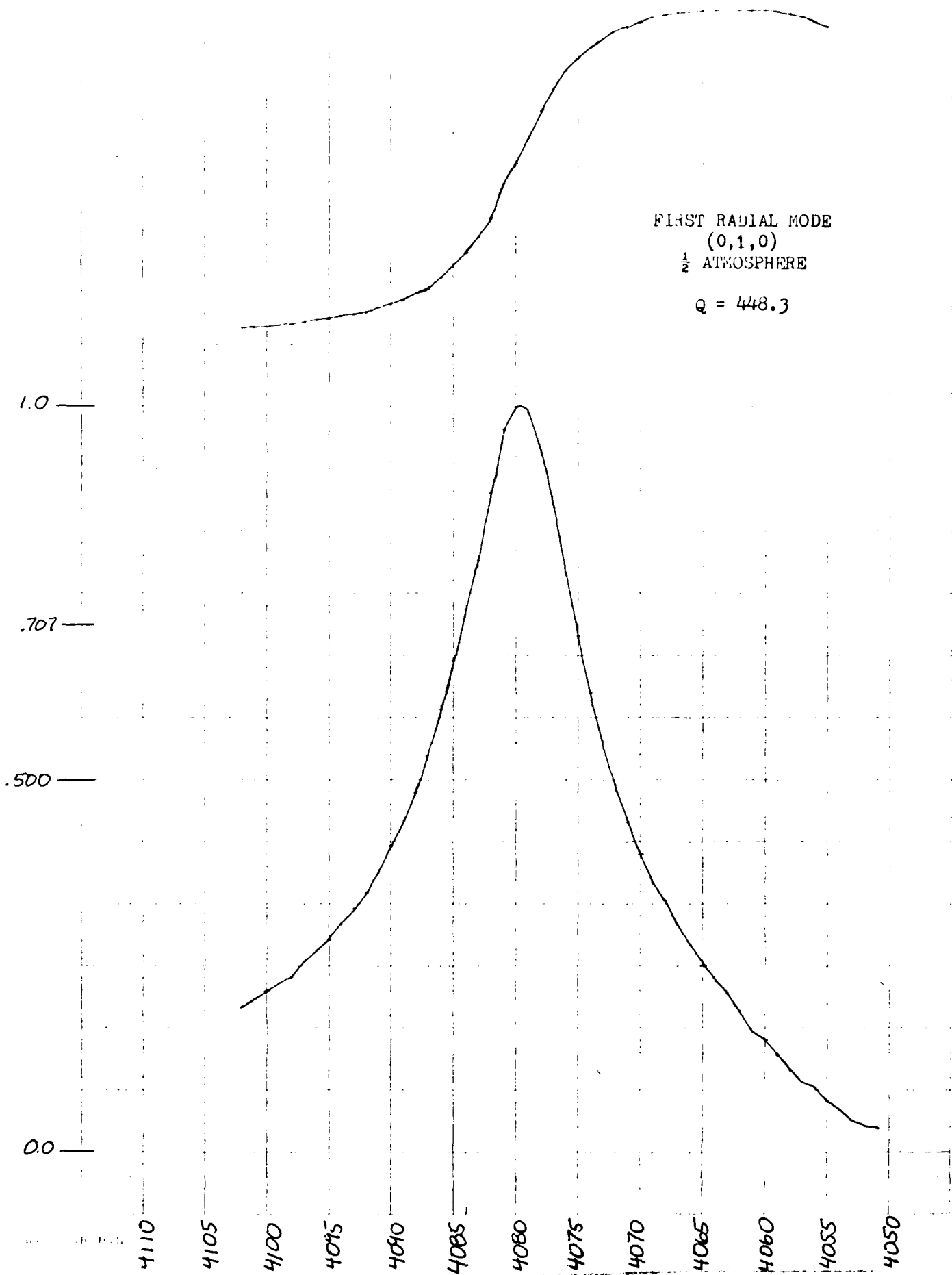
4070

4065

4060

4055

4050



REFERENCES

1. Morse, P.M. and Ingard, K.U. Theoretical Acoustics, McGraw-Hill, New York, 1968.
2. Dewey, C.F.; Kamm, R.D.; and Hackett, C.E. "Acoustic Amplifier for Detection of Atmospheric Pollutants," Appl. Phys. Lett., Vol. 23, No. 11, 1 Dec 1973.
3. Thomas, L.J.; Kelly, M.J.; and Amer, N.M. "The Role of Buffer Gases in Optoacoustic Spectroscopy," Appl. Phys. Lett., Vol. 32, No. 11, 1 Jun 1978.
4. Parker, J.G. and Ritke, D.N. "Collisional Deactivation of Vibrationally Excited Singlet Molecular Oxygen," J. Chem. Phys., Vol. 59, No. 7, 1 Oct 1973.
5. Shumate, M.S.; Menzies, R.T.; Margolis, J.S.; and Rosengren, L.-G. "Water Vapor Absorption of Carbon Dioxide Laser Radiation," Appl. Optics, Vol. 15, No. 10, Oct 1976.
6. Bienkowski, G.K. "The Acoustics in Photo-Acoustic Spectroscopy," Unpublished.
7. Dewey, C.F. "Design of Optoacoustic Systems," in Optoacoustic Spectroscopy and Detection, Y.H. Pao ed., Academic Press, New York, 1977.
8. Stettler, J.D. and Witriol, N.M. "Energy Transfer Mechanisms," in Optoacoustic Spectroscopy and Detection, Y.H. Pao ed., Academic Press, New York, 1977.
9. Goldan, P.D. and Goto, K. "An Acoustically Resonant System for Detection of Low Level Infra-red Absorption in Atmospheric Pollutants," J. Appl. Phys., Vol. 45, No. 10, Oct 1974.
10. Kreuzer, L.B. "The Physics of Signal Generation and Detection," in Optoacoustic Spectroscopy and Detection, Y.H. Pao ed., Academic Press, New York, 1977.
11. Morse, P.M. and Ingard, K.U. Handbuch Der Physik, S. Flugge ed., Vol. XI/1, Springer-Verlag, Berlin, 1961.
12. Kamm, R.D. "Detection of Weakly Absorbing Gases Using a Resonant Optoacoustic Method," J. Appl. Phys., Vol. 47, No. 8, Aug 1976.
13. Rosengren, L.-G. "Optimal Optoacoustic Detector Design," Appl. Optics, Vol. 14, No. 8, Aug. 1975.
14. Kerr, E.L. and Atwood, J.G. "Laser Illuminated Absorptivity Spectrophone:," Appl. Optics, Vol. 7, No. 5, May 1968.

15. Kreuzer, L.B. "Ultralow Gas Concentration Infra-red Absorption Spectroscopy," J. Appl. Phys., Vol. 42, No. 7, June 1971.
16. Koch, K.P. and Lahmann, W. "Optoacoustic Detection of Sulphur Dioxide Below the Parts per Billion Level," Appl. Phys. Lett., Vol. 32, No. 5, 1 March 1978.
17. Harshberger, W.R. and Robin, M.B. "The Opto-Acoustic Effect: Revival of an Old Technique for Molecular Spectroscopy," Accts. of Chem. Res., Vol. 6, No. 10, October 1973.
18. Angus, A.M.; Marinero, E.E.; Colles, M.J. "Opto-Acoustic Spectroscopy With a Visible CW Dye Laser," Optics Commun., Vol. 14, No. 2, June 1975.